Spectroscopic detection and kinetic analysis of short-lived aromatic amine cation radicals using an electron transfer stopped-flow method

Munetaka Oyama,*[a,b] Toshihiro Higuchi[b] and Satoshi Okazaki[b]

[a] *Division of Creative Research, International Innovation Center, Kyoto University, Sakyo-ku, Kyoto 606-8501, Japan. E-mail: oyama@iic.kyoto-u.ac.jp; Fax: +81-75-761-8846; Tel: +81-75-753-5885*

[b] *Department of Material Chemistry, Graduate School of Engineering, Kyoto University, Sakyo-ku, Kyoto 606-8501, Japan*

Received (in Cambridge, UK) 2nd May 2001, Accepted 31st May 2001
First published as an Advance Article on the web 25th June 2001

Using an electron transfer stopped-flow (ETSF) method, the reactions of short-lived methyldiphenylamine and diphenylamine cation radicals ($MDPA^{\bullet+}$ and $HDPA^{\bullet+}$) in acetonitrile (AN) were analysed by generating them quantitatively by electron transfer with tris(*p*-bromophenyl)amine cation radical ($TBPA^{\bullet+}$). The absorption spectra of short-lived $MDPA^{\bullet+}$ and $HDPA^{\bullet+}$ could be successfully observed in a time frame of less than a few tens of milliseconds using a rapid-scan spectrophotometer, and as a result, the kinetics of the dimerization reaction could be analyzed in spite of the follow-up oxidation reactions of the dimer compounds, which are affected by the concentration of the neutral monomer. Both reactions are found to be second order in concentration of cation radicals, and the dimerization rate constants were determined to be 1.4×10^6 M^{-1} s^{-1} for $MDPA^{\bullet+}$, and 1.0×10^6 M^{-1} s^{-1} for $HDPA^{\bullet+}$. Compared with electrochemical methods, the ETSF method permits direct detection and straightforward kinetic analysis of short-lived cation radicals, as well as the elucidation of the effect of precursor molecules on subsequent reactions.

Introduction

Numerous studies have already been devoted to the reaction kinetics of electrogenerated cation radicals,[1–4] and it is still an area of active research.[5] In a recent review by Schmittel and Burghart, various aspects of the reactions of cation radicals have been well summarized.[6]

By developing a pulse-electrolysis stopped-flow (PESF) method,[7] we have been contributing to the kinetic analysis of electrogenerated cation radicals with nucleophiles.[8–13] In the PESF method, synchronized with pulse-electrolysis using a carbon wool working electrode, an electrolyzed solution is delivered to an optical cell by a piston drive, and then spectroscopic measurements can be carried out after stopping the solution.[7] Alternatively, by mixing the electrolyzed solution with a solution containing nucleophiles, kinetic analysis can be performed in a manner similar to the conventional stopped-flow technique.[7] It is advantageous that the reactions of the electrogenerated species can be analyzed in homogeneous solutions separately from electrode phenomena.

This method has also been utilized in the analysis of electron and energy transfer reactions between cation and anion radicals from different precursors in acetonitrile (AN) by observing electrogenerated chemiluminescence. For this purpose, a dual electrolysis stopped-flow method was developed and applied utilizing the principle of the PESF method.[14,15]

However, in the PESF method, a serious problem remains for the generation, observation and analysis of short-lived electrogenerated species. Namely, although column electrolysis using a carbon wool working electrode permits quantitative electrolysis within several tens of milliseconds, spectrochemical observation is impossible for short-lived species that diminish during the minimized time of pulse electrolysis.

To overcome this problem, we have proposed the novel concept of an electron transfer stopped-flow (ETSF) method in a recent communication.[16] In the ETSF method, for example, unstable cation radicals ($N^{\bullet+}$) are formed *via* electron transfer with long-lived cation radicals ($M^{\bullet+}$). That is to say, when the redox potential of the $M^{\bullet+}/M$ couple is positive relative to that of the $N^{\bullet+}/N$ couple, the electron transfer reaction of eqn. (1)

$$N + M^{\bullet+} \longrightarrow N^{\bullet+} + M \qquad (1)$$

should be thermodynamically favorable. Thus, by mixing the solutions of N and $M^{\bullet+}$, we can form $N^{\bullet+}$ *via* eqn. (1) and initiate the reaction of $N^{\bullet+}$. Consequently, the dead time from the point of the generation of cation radicals to the point for the optical measurement can be reduced dramatically.

Such formation of cation radicals by other cation radicals is well known,[17] and the correlation between redox equilibria and potential has been investigated previously.[18] Nevertheless, it can be emphasized that, by combining the electron transfer reactions with a stopped-flow operation, spectroscopic measurements for short-lived intermediates which have never before been investigated now become possible, in particular, with the help of the recent development of a rapid-scan spectrophotometer.

In our previous communication, we proposed the concept of the ETSF method with some examples of cation radicals of the phenylamine derivatives, methyldiphenylamine (MDPA) and diphenylamine (HDPA) in AN.[16] It is well known that triphenylamine cation radical ($TPA^{\bullet+}$) dimerizes to form the product tetraphenylbenzidine (TPB) in AN.[19,20] For much shorter-lived aromatic amine cation radicals, using ultramicroelectrode voltammetry, Larumbe *et al.* analyzed the dimerization reaction of dimethylaniline cation radical ($DMA^{\bullet+}$) and reported a second-order rate constant of 1.5×10^7 M^{-1} s^{-1}.[21] Also, using rapid-scan cyclic voltammetry, Yang and Bard analyzed the dimerization reaction of HDPA cation radical

DOI: 10.1039/b103921k

($HDPA^{\bullet+}$) in AN, whose reaction rate was reported to be 2.0×10^5 M^{-1} s^{-1}.[22] The cation radicals of diphenylamine derivatives are thus expected to be less reactive than $DMA^{\bullet+}$, and hence, the measurement of the absorption spectra of $MDPA^{\bullet+}$ and $HDPA^{\bullet+}$ can be targeted in analysis using the ETSF method.

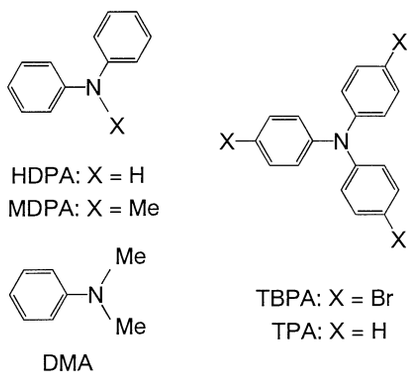

The aim of the present paper is to describe the details of the spectroscopic detection and kinetic analysis of short-lived $MDPA^{\bullet+}$ and $HDPA^{\bullet+}$ using the ETSF method, together with the results for $TPA^{\bullet+}$. In particular, we want to demonstrate that the ETSF method permits straightforward analysis of kinetic processes by observation of the changes in absorption spectra. In addition, as one of the advantages of the ETSF method is that the reaction analysis is carried out in homogeneous solution, the effects of precursor molecules on the subsequent electron transfer reactions can be shown.

Experimental

For the stopped-flow measurements, a rapid-scan stopped-flow spectroscopic system, RSP-601 (Unisoku Co. Ltd., Hirakata, Japan), was used. In this apparatus, dynamic transformation of absorption spectra can be observed with a minimized time interval of 1.0 ms after mixing of the two solutions. All the measurements were carried out in AN as a solvent.

As a substrate to form persistent cation radicals [$M^{\bullet+}$, in eqn. (1)] we used tris(*p*-bromophenyl)amine (TBPA), which is known to form a very long-lived cation radical in AN,[23,24] due to the bromo-substituents that make the oxidation potential of $TBPA^{\bullet+}$ positive relative to that of TPA.[25] Because $TBPA^{\bullet+}$ is long-lived enough to survive over several days in AN and is less reactive towards water, AN solutions of $TBPA^{\bullet+}$ were prepared by a conventional batchwise electrolysis. The $TBPA^{\bullet+}$ solution was used after adjusting its concentration by dilution with AN. The concentration of $TBPA^{\bullet+}$ was determined by the absorption measurement using the molar absorptivity of $TBPA^{\bullet+}$ at 705 nm, $\varepsilon = 3.2 \times 10^4$ M^{-1} cm^{-1}.[23] In the present ETSF experiments, the AN solution of $TBPA^{\bullet+}$ was mixed with an AN solution containing the aromatic amine derivatives, MDPA, HDPA or TPA.

For all the substrates, chemicals of the highest purity available were used as received. For the solvent, dehydrated acetonitrile (Wako chemicals) was used as received. As the supporting electrolyte used in the batchwise electrolysis, tetrabutylammonium perchlorate (TBAP) was used. It was prepared from tetrabutylammonium bromide (Aldrich) and $NaClO_4$ (Nacalai Tesque, GR grade), and then purified by three separate recrystallizations from ethanol–water.

Results and discussion

Electrochemical aspects of electron transfer in the present reaction systems

To bring about the electron transfer shown in eqn. (1), we adopted $TBPA^{\bullet+}$ as $M^{\bullet+}$. Fig. 1A shows the cyclic voltammogram (CV) of TBPA in AN, which shows that this one-electron oxidation process is reversible. As mentioned in the Experimental section, $TBPA^{\bullet+}$ is fairly long-lived in AN, so the absorption spectrum was observed easily. The obtained absorption spectrum was identical to that reported previously,[23,24] which has an absorption maximum at 705 nm.

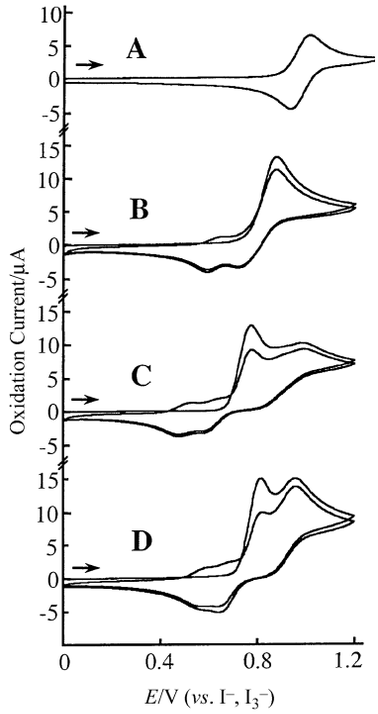

Fig. 1 Cyclic voltammograms of aromatic amines in AN. (A) TBPA, (B) TPA, (C) MDPA and (D) HDPA. Working electrode: Pt disk electrode (diam. 1.6 mm). Reference electrode: Pt/(I^-,I_3^-) electrode. Scan rate; 100 mV s^{-1}. Concentration of amine: 1.0 mM. TBAP: 0.10 M.

Fig. 1B–D shows the CVs of the aromatic amine derivatives, TPA, MDPA and HDPA, which we adopted as N to form the unstable $N^{\bullet+}$ in eqn. (1). As is well known, reversible waves are not observed for these aromatic amines at a scan rate of 100 mV s^{-1}, but the reduction waves of the dimer compounds, *N*,*N*′-diphenylbenzidine derivatives, were observed in the CVs.[7,19,21,22]

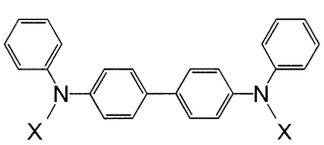

The reaction process can be summarized as follows [eqns. (2)–(4)], for TPA as an example.

$$TPA \overset{-e^-}{\rightleftharpoons} TPA^{\bullet+} \quad (2)$$

$$2TPA^{\bullet+} \longrightarrow TPB + 2H^+ \quad (3)$$

$$TPB \overset{-e^-}{\rightleftharpoons} TPB^{\bullet+} \overset{-e^-}{\rightleftharpoons} TPB^{2+} \quad (4)$$

The two-step reductions in the cathodic scans can be attributed to the reduction of the benzidines formed, as represented by eqn. (4). The oxidation peaks observed in the potential region positive to the oxidation of the amines in Figs. 1C and D

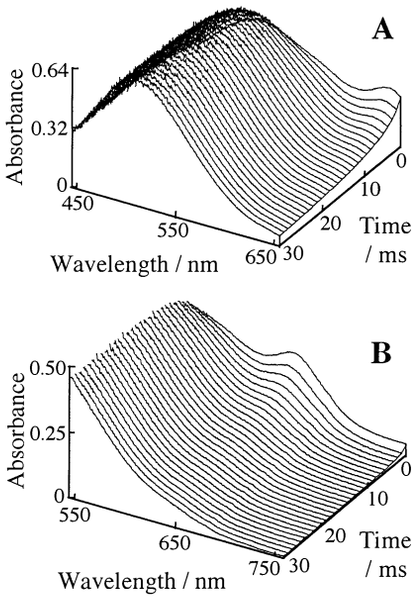

Fig. 2 Dynamic transformation of absorption spectra recorded after an AN solution of 0.12 mM MDPA was mixed with an AN solution of 0.12 mM $TBPA^{\bullet+}$. Observed wavelength region: (A) 445–655 nm, (B) 545–755 nm. Time interval between each spectrum: 1.0 ms.

can be assigned to the oxidation of the protonated form of aromatic amine monomers.[22,26]

In spite of the irreversibility and the complexity of the CVs for these three aromatic amines, judging from the oxidation potentials summarized in Fig. 1, the electron transfer reactions with $TBPA^{\bullet+}$ in eqns. (5)–(7) should be thermodynamically

$$TPA + TBPA^{\bullet+} \longrightarrow TPA^{\bullet+} + TBPA \quad (5)$$

$$MDPA + TBPA^{\bullet+} \longrightarrow MDPA^{\bullet+} + TBPA \quad (6)$$

$$HDPA + TBPA^{\bullet+} \longrightarrow HDPA^{\bullet+} + TBPA \quad (7)$$

favorable because the redox potential of the $TBPA^{\bullet+}$/TBPA couple is positive relative to those of the others.

Spectroscopic detection of $MDPA^{\bullet+}$ using the ETSF method

First, the effective features of the ETSF method for the spectroscopic detection and kinetic analysis of short-lived aromatic amine cation radicals are demonstrated in the case of $MDPA^{\bullet+}$.

When $TBPA^{\bullet+}$ is mixed with an equimolar amount of MDPA, the electron transfer shown in eqn. (6) should occur to form $MDPA^{\bullet+}$ quantitatively. In addition, if the electron transfer shown in eqn. (6) is a diffusion-controlled reaction, one would expect that the electron transfer reaction should be completed in the mixing part of the stopped-flow apparatus before reaching the part for the optical measurements.

Fig. 2A shows the dynamic transformation of the absorption spectra observed in the ETSF method after an AN solution of 0.12 mM MDPA was mixed with an AN solution of 0.12 mM $TBPA^{\bullet+}$. It is clearly shown that the absorption maximum at 639 nm decreased within several milliseconds after stopping the solution. The spectrophotometer has an observable wavelength region width of 210 nm, so a second observed region is shown in Fig. 2B. This figure shows that the absorption maximum of $TBPA^{\bullet+}$ at 705 nm disappears completely, even just after the mixing, though it is observed when the $TBPA^{\bullet+}$ solution was mixed with AN only.

From these results, we established that the absorption spectrum of short-lived $MDPA^{\bullet+}$ had been successfully recorded using the ETSF method by bringing about the electron transfer reaction shown in eqn. (6) during the mixing of the solutions.

The absorption spectrum of $MDPA^{\bullet+}$ has been reported; it was previously prepared using a photo-oxidation method in glass matrices at low temperatures.[27,28] The present result clearly demonstrates that the absorption spectrum of such short-lived intermediates can be observed using the ETSF method, *via* their generation by diffusion-controlled electron transfer. In addition, on the basis of this principle, it is expected that that the dynamic aspects of the decay kinetics could be analyzed.

Dimerization of $MDPA^{\bullet+}$ and subsequent electron transfer reactions

For a comprehensive analysis of the dimerization process of $MDPA^{\bullet+}$ the decay kinetics can be analyzed by following the decay of $MDPA^{\bullet+}$ at 639 nm, and the increase in absorption around 500 nm in Fig. 2A should be discussed. In the dimerization reaction of $MDPA^{\bullet+}$, *N*,*N*′-dimethyl-*N*,*N*′-diphenylbenzidine (DMDPB) is formed *via* eqn. (8). Furthermore, in

$$2MDPA^{\bullet+} \xrightarrow{k} DMDPB + 2H^{+} \quad (8)$$

homogeneous solution, even in the absence of the electrode, DMDPB should oxidized by $MDPA^{\bullet+}$ to $DMDPB^{\bullet+}$ and further to $DMDPB^{2+}$ *via* eqns. (9) and (10) as shown by the CV

$$DMDPB + MDPA^{\bullet+} \underset{}{\overset{K_1}{\rightleftharpoons}} DMDPB^{\bullet+} + MDPA \quad (9)$$

$$DMDPB^{\bullet+} + MDPA^{\bullet+} \underset{}{\overset{K_2}{\rightleftharpoons}} DMDPB^{2+} + MDPA \quad (10)$$

(Fig. 1C), because the redox potentials of the $DMDPB^{\bullet+}$/DMDPB and $DMDPB^{2+}$/$DMDPB^{\bullet+}$ couples are negative relative to that of $MDPA^{\bullet+}$/MDPA [eqn. (11)].

$$E(DMDPB^{\bullet+}/DMDPB) < E(DMDPB^{2+}/DMDPB^{\bullet+}) < E(MDPA^{\bullet+}/MDPA) \quad (11)$$

However, compared with the dimerization reaction [eqn. (8)], the electron transfer reactions shown by eqns. (9) and (10) should be very rapid [like the reaction shown in eqn. (6)] because they are diffusion-controlled reactions driven thermodynamically. Thus, in the kinetic analysis, it is important to observe the rate-determining decay process of $MDPA^{\bullet+}$ in eqn. (8). Even though $MDPA^{\bullet+}$ is formed in the reversed reactions of eqns. (9) and (10), it should be converted *via* eqn. (8) to the oxidation states of DMDPB during the progress of the reactions, and eventually become negligible. The decrease of $MDPA^{\bullet+}$ to a negligible amount was confirmed by regressive calculations. This is also in agreement with the result of the decay of $MDPA^{\bullet+}$ (shown later).

While neutral DMDPB has no absorption in the visible region, $DMDPB^{\bullet+}$ and $DMDPB^{2+}$ have absorption maxima at 476 and 512 nm, respectively.[29] Judging from the wavelengths and molar absorptivities for $DMDPB^{\bullet+}$ ($\varepsilon = 2.3 \times 10^4$ M^{-1} cm^{-1}, at 476 nm) and $DMDPB^{2+}$ ($\varepsilon = 3.5 \times 10^4$ M^{-1} cm^{-1}, at 512 nm),[29] it is ascertained that $DMDPB^{2+}$ was the major product in the reaction between 0.12 mM $TBPA^{\bullet+}$ and 0.12 mM MDPA (Fig. 2A).

In order to analyze in detail the equilibria brought about by subsequent electron transfer reactions [eqns. (9) and (10)] after the formation of DMDPB [eqn. (8)], we next observe the effect of the concentration of the precursor MDPA on the dynamic transformation of the absorption spectra.

Effect of MDPA on the oxidation states of DMDPB

Fig. 3 shows the effect of the precursor, MDPA, on the dynamic transformation of the absorption spectra. The AN solution of 0.12 mM $TBPA^{\bullet+}$ was mixed with AN solutions containing 1.2 and 12 mM MDPA in Figs. 3A and B, respectively.

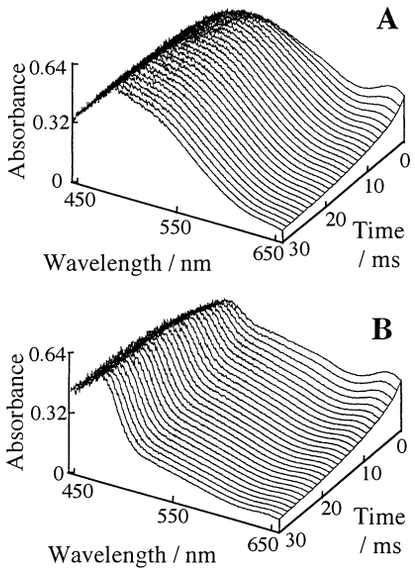

Fig. 3 Effect of MDPA concentration on the dynamic transformation of absorption spectra recorded after an AN solution of MDPA was mixed with an AN solution of 0.12 mM $TBPA^{\bullet+}$. Concentration of MDPA: (A) 1.2 and (B) 12 mM. Observed wavelength region: 445–655 nm. Time interval between each spectrum: 1.0 ms.

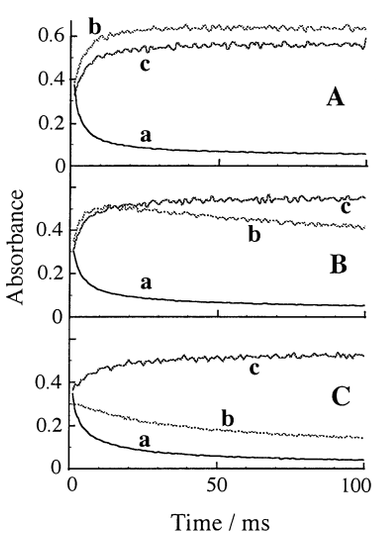

Fig. 4 Time changes in absorbance at (a) 639, (b) 512 and (c) 476 nm for 100 ms after an AN solution of MDPA was mixed with an AN solution of 0.12 mM $TBPA^{\bullet+}$. The wavelengths correspond to the absorption maxima of (a) $MDPA^{\bullet+}$, (b) $DMDPB^{2+}$ and (c) $DMDPB^{\bullet+}$, respectively. Concentration of MDPA: (A) 0.12, (B) 1.2 and (C) 12 mM.

By comparing Figs. 2A, 3A and 3B, it is apparent that the absorption around 500 nm was significantly affected by the concentration of MDPA. To see the changes in the absorption spectra in detail, Fig. 4 shows changes in absorbance with time at (a) 639, (b) 512 and (c) 476 nm, which correspond to the absorption maxima of $MDPA^{\bullet+}$, $DMDPB^{2+}$ and $DMDPB^{\bullet+}$, respectively.

Remarkably, from the curves (a) in Fig. 4, the decay kinetics of $MDPA^{\bullet+}$ are shown to be unaffected by MDPA, even when it is in large excess. This indicates that the dimerization reaction does not proceed *via* a cation radical–parent coupling, but *via* the cation radical–cation radical coupling mechanism common to aromatic amine cation radicals.[6,21,22]

However, the final oxidation state of the formed dimer, DMDPB, is seen to be dependent on the concentration of MDPA. Judging from the absorption spectra of $DMDPB^{\bullet+}$ and $DMDPB^{2+}$,[29] $DMDPB^{\bullet+}$ is the major product in the reaction between 0.12 mM $TBPA^{\bullet+}$ and 12 mM MDPA, while the major product in the reaction with 0.12 mM MDPA is $DMDPB^{2+}$.

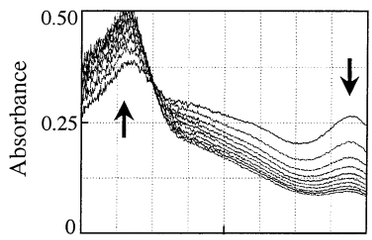

Fig. 5 Dynamic transformation of absorption spectra displayed in two dimensions. Transformation observed just after an AN solution of 12 mM MDPA was mixed with an AN solution of 0.12 mM $TBPA^{\bullet+}$. Time interval between each spectrum: 2.0 ms.

These differences can be reasonably deduced from eqns. (8)–(11). When the concentration of neutral MDPA is increased, it should suppress the oxidation of DMDPB, in particular, the oxidation to $DMDPB^{2+}$. Thus, it can be concluded that the absorption spectra change reflecting the ratio of $MDPA^{\bullet+}$/MDPA. Under conditions where MDPA is totally oxidized to $MDPA^{\bullet+}$ by $TBPA^{\bullet+}$ (*i.e.* in the reaction between 0.12 mM $TBPA^{\bullet+}$ and 0.12 mM MDPA), $DMDPB^{2+}$ is the major product because there is less MDPA to reduce it. The overall reaction thus can be expressed as eqn. (12).

$$4MDPA^{\bullet+} \longrightarrow DMDPB^{2+} + 2MDPA + 2H^{+} \quad (12)$$

On the other hand, under conditions where MDPA is in large excess of $TBPA^{\bullet+}$ (*i.e.* in the reaction between 0.12 mM $TBPA^{\bullet+}$ and 12 mM MDPA), the overall reaction is thought to be expressed by eqn. (13).

$$3MDPA^{\bullet+} \longrightarrow DMDPB^{\bullet+} + MDPA + 2H^{+} \quad (13)$$

The simplicity of both overall reactions could also be confirmed by the existence of the isosbestic points. The isosbestic point observed in the latter case is shown in Fig. 5.

Kinetic analysis of the dimerization reaction of $MDPA^{\bullet+}$

In spite of the complex equilibria after forming DMDPB, it is expected that the reaction kinetics of the dimerization reaction [eqn. (8)] are very simple. This is because the decay curves of $MDPA^{\bullet+}$ were almost identical, independent of the concentration of MDPA. Judging from the curves (a) and (b) in Fig. 4A, the curves (a) and (c) in Fig. 4C, and the fact that isosbestic points were observed, the electron transfer reactions to form $DMDPB^{2+}$ or $DMDPB^{\bullet+}$ are assumed to be much faster than the dimerization reaction of eqn. (8). Therefore, the rate determining reaction constant, k, in eqn. (8) can be determined simply from Fig. 4A (a) and (c).

That means, comparing the increase in $DMDPB^{2+}$ with the decrease in $MDPA^{\bullet+}$, the molar absorptivity of $MDPA^{\bullet+}$ can be estimated to be 8.5×10^3 M^{-1} cm^{-1} at 639 nm on the basis of eqn. (12). By converting the absorbance into the concentration using this value, in Fig. 6, digital simulation analysis was performed for decay curve (a) in Fig. 4.

As a result, the decay reaction was found to be second order in $[MDPA^{\bullet+}]$ as shown in Fig. 6. This indicates that the reaction proceeds *via* a cation radical–cation radical coupling reaction. In addition, from the excellent fitting of Fig. 6 curves (a) and (b), the second-order rate constant was determined to be 1.4×10^6 M^{-1} s^{-1} by taking into account that four $MDPA^{\bullet+}$s are consumed in the overall reaction shown by eqn. (12). In this case, the contribution of $DMDPB^{2+}$ to the absorbance at 639 nm was negligible in analyzing the dimerization reaction of $MDPA^{\bullet+}$.

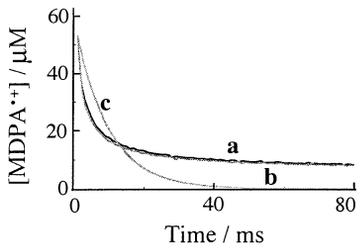

Fig. 6 (a) Time decay curve of $MDPA^{\bullet+}$ (black line). The concentration of $MDPA^{\bullet+}$ was determined as described in the text from the absorbance at 639 nm. The source is Fig. 4A (a). (b) Result of the simulation assuming a second-order decay reaction of $MDPA^{\bullet+}$ (gray line). (c) Result of the simulation supposing a first order decay reaction of $MDPA^{\bullet+}$ (gray line) with a rate constant of 100 s^{-1}.

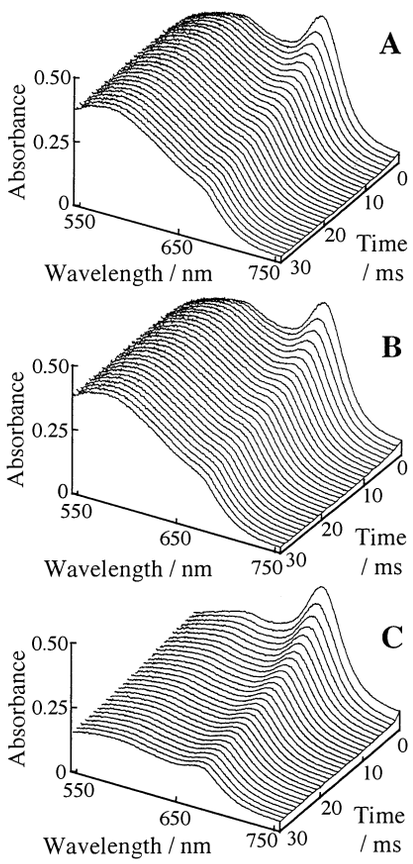

Fig. 7 Effect of HDPA concentration on the dynamic transformation of absorption spectra recorded after an AN solution of HDPA was mixed with an AN solution of 0.12 mM $TBPA^{\bullet+}$. Concentration of HDPA: (A) 0.12, (B) 1.2 and (C) 12 mM. Observed wavelength region: 545–755 nm. Time interval between each spectrum: 1.0 ms.

Dimerization reaction of $HDPA^{\bullet+}$

Next, we analyzed the dimerization reaction of $HDPA^{\bullet+}$. Before the analysis using the ETSF, the absorption spectra of the oxidized states of the dimer compound, *N*,*N*′-diphenylbenzidine (DHDPB) were measured using a column-electrolysis continuous flow method.[29] While neutral DHDPB has no absorption in the visible region, $DHDPB^{\bullet+}$ and $DHDPB^{2+}$ are confirmed to have absorption maxima at 490 ($\varepsilon = 1.3 \times 10^4$ M^{-1} cm^{-1}) and 575 nm ($\varepsilon = 2.4 \times 10^4$ M^{-1} cm^{-1}), respectively.

Fig. 7A shows the dynamic transformation of the absorption spectra obtained after mixing AN solutions of 0.12 mM HDPA and 0.12 mM $TBPA^{\bullet+}$. As in the case of MDPA, the absorption spectrum of $HDPA^{\bullet+}$, whose absorption maximum is 675 nm,

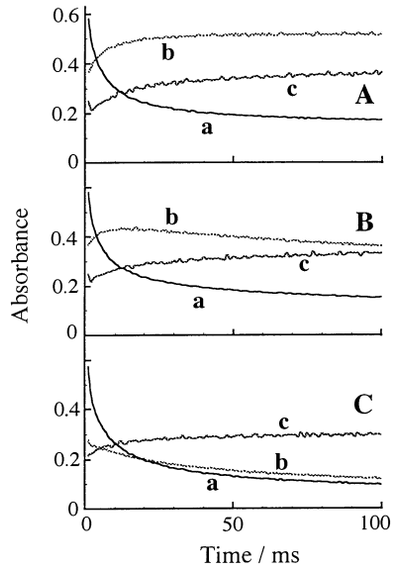

Fig. 8 Time changes in absorbance at (a) 675, (b) 575 and (c) 490 nm for 100 ms after an AN solution of HDPA was mixed with an AN solution of 0.12 mM $TBPA^{\bullet+}$. The wavelengths correspond to the absorption maxima of (a) $HDPA^{\bullet+}$, (b) $DHDPB^{2+}$, and (c) $DHDPB^{\bullet+}$, respectively. Concentration of HDPA: (A) 0.12, (B) 1.2 and (C) 12 mM.

could be detected. The absorption maximum is in good agreement with those measured in the glass matrices.[27,28]

Figs. 7B and C show the results obtained after mixing 0.12 mM $TBPA^{\bullet+}$ with 1.2 and 12 mM HDPA, respectively. The wavelength region shown in Fig. 7 is 545–755 nm; the formation of $DHDPB^{\bullet+}$ could be observed in the wavelength region around 490 nm, in particular, under the conditions used for Fig. 7C. Fig. 8 shows the changes in absorbance at 675, 575 and 490 nm, which correspond to the absorption maxima of $HDPA^{\bullet+}$, $DHDPB^{2+}$ and $DHDPB^{\bullet+}$, respectively.

From these results, as a general conclusion for the dimerization reaction of $HDPA^{\bullet+}$, it was confirmed that the chemical aspects were very similar to those of $MDPA^{\bullet+}$. The overall reactions are thus expressed by eqn. (14) for the reaction between 0.12 mM $TBPA^{\bullet+}$ and 0.12 mM HDPA, and eqn. (15) for the reaction of 0.12 mM $TBPA^{\bullet+}$ with 12 mM HDPA.

$$4HDPA^{\bullet+} \longrightarrow DHDPB^{2+} + 2HDPA + 2H^{+} \quad (14)$$

$$3HDPA^{\bullet+} \longrightarrow DHDPB^{\bullet+} + HDPA + 2H^{+} \quad (15)$$

From the decay kinetics of $HDPA^{\bullet+}$, from Figs. 7 and 8 one would expect the dimerization reaction rate of $HDPA^{\bullet+}$ to be a little slower than that of $MDPA^{\bullet+}$. However, to precisely determine the rate constant of $HDPA^{\bullet+}$ some correction is necessary, in contrast to the case of $MDPA^{\bullet+}$, because the overlap of the absorption between $HDPA^{\bullet+}$ and $DHDPB^{2+}$ was significant in Fig. 7A. The correction procedure is shown in Fig. 9. Because the oxidation to $DHDPB^{2+}$ after the dimerization is sufficiently rapid, the molar absorption coefficient of $HDPA^{\bullet+}$ could be estimated to be 1.2×10^4 M^{-1} cm^{-1} at 675 nm by eliminating the contribution of $DHDPB^{2+}$. For the corrected decay curve Fig. 9c excellent agreement was obtained by assuming the second-order decay of $HDPA^{\bullet+}$ as shown in Fig. 9d. As a result, the second-order rate constant was determined to be 1.0×10^6 M^{-1} s^{-1} by taking into account that four $HDPA^{\bullet+}$s are consumed in the overall reaction shown by eqn. (14). This value is slightly larger than the value reported using rapid-scan voltammetry.[22]

Dimerization reaction of $TPA^{\bullet+}$

Finally, the well-known dimerization reaction of $TPA^{\bullet+}$ was

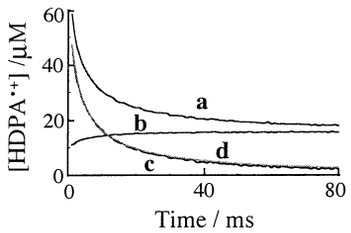

Fig. 9 (a) Time decay curve of $HDPA^{\bullet+}$ directly obtained from Fig. 8A (a) using the estimated molar absorption coefficient of $HDPA^{\bullet+}$. (b) Estimate of the contribution of $DHDPB^{2+}$ to the absorbance at 675 nm, which was determined to be *ca.* 30% of Fig. 8A (b). (c) Corrected time decay curve of $HDPA^{\bullet+}$ calculated by removing the contribution to the absorption of $DHDPB^{2+}$, *i.e.* the concentration was determined as curve (a) minus curve (b) (black line). (d) Result of the simulation assuming a second order decay reaction of $HDPA^{\bullet+}$ (gray line).

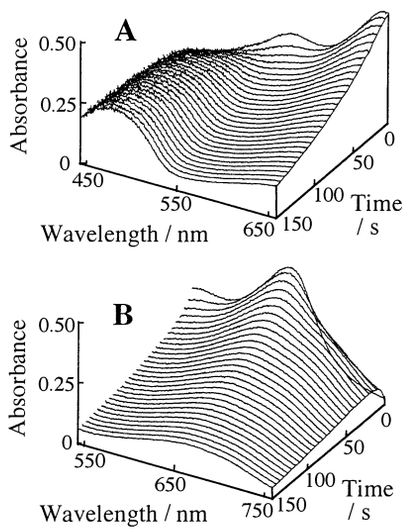

Fig. 10 Dynamic transformation of absorption spectra recorded after an AN solution of 0.12 mM TPA was mixed with an AN solution of 0.12 mM $TBPA^{\bullet+}$. Observed wavelength region: (A) 445–655 nm, (B) 545–755 nm. Time interval between each spectrum: 5 s.

analysed using the ETSF method. Compared with the reactions of $MDPA^{\bullet+}$ and $HDPA^{\bullet+}$, the reaction of $TPA^{\bullet+}$ seems very slow, though we had used this reaction for describing the PESF method previously.[7]

Fig. 10 shows the dynamic transformation of the absorption spectra observed using the ETSF method after an AN solution of 0.12 mM TPA was mixed with an AN solution of 0.12 mM $TBPA^{\bullet+}$. Please note that the time interval of each absorption spectrum is 5.0 s, whereas it was 1.0 ms for $MDPA^{\bullet+}$ and $HDPA^{\bullet+}$. This difference would be deduced from the rate constants; 1.8×10^3 M^{-1} s^{-1} for $TPA^{\bullet+}$,[7] 1.4×10^6 M^{-1} s^{-1} for $MDPA^{\bullet+}$, and 1.0×10^6 M^{-1} s^{-1} for $HDPA^{\bullet+}$.

While the dimer dication was quantitatively formed in the reactions between 0.12 mM $TBPA^{\bullet+}$ and 0.12 mM MDPA, or HDPA, the final oxidized state in the case of TPA was found to contain both $TPB^{\bullet+}$ and TPB^{2+}, whose absorption maxima are 480 and 680 nm, respectively.[7] In addition, from the changes in absorbance with time (Fig. 11), it was clarified that TPB^{2+} was generated firstly just after mixing, and then $TPB^{\bullet+}$ increased gradually with decreasing TPB^{2+} and $TPA^{\bullet+}$.

The reason of this behavior can be attributed to the difference in the redox potentials between *E*(monomer cation radical/monomer) and *E*(dimer dication/dimer cation radical). As seen in Fig. 1, the difference between *E*($TPA^{\bullet+}$/TPA) and *E*(TPB^{2+}/$TPB^{\bullet+}$) is apparently smaller than the analogous values for MDPA and HDPA. Thus, it is to be expected that, once formed, TPB^{2+} is reduced to $TPB^{\bullet+}$, reflecting the ratio of $TPA^{\bullet+}$/TPA that changes during the course of the consecutive electron

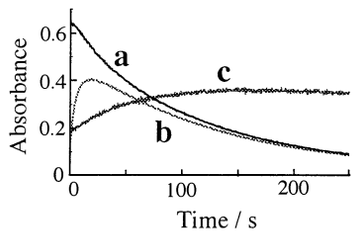

Fig. 11 Time changes in absorbance at (a) 647, (b) 680 and (c) 480 nm for 250 s after an AN solution of 0.12 mM TPA was mixed with an AN solution of 0.12 mM $TBPA^{\bullet+}$. The wavelengths correspond to the absorption maxima of (a) $TPA^{\bullet+}$, (b) TPB^{2+} and (c) $TPB^{\bullet+}$, respectively.

transfer reactions, even when $TPA^{\bullet+}$ is generated quantitatively on mixing with an equimolar amount of $TBPA^{\bullet+}$.

Therefore, in the ETSF method, it can be concluded that particular attention should be paid to the follow-up chemical reactions and equilibria for complex reaction systems, such as the ones described here. However, this also means that comprehensive studies on reactions and equilibria in solution are now possible using the ETSF method, by initiating the formation of starting intermediates. In addition, it is a characteristic of the method that such observations can be performed in completely homogeneous solutions, which is a significant difference from other electrochemical methods.

Conclusions

Using the ETSF method, the detection and kinetic analysis of the short-lived aromatic amine cation radicals, $MDPA^{\bullet+}$ and $HDPA^{\bullet+}$, could be successfully carried out. The absorption spectra of these cation radicals could be observed at room temperature for the first time. In addition, from the excellent fits with the results of simulations, it was found that the decay reactions of $MDPA^{\bullet+}$ and $HDPA^{\bullet+}$ were second order in cation radicals. This confirms that the reactions proceed through a cation radical–cation radical coupling mechanism; this has been proved previously by an electrochemical method.[21,22]

Compared with electrochemical methods, the present spectroscopic analysis in homogeneous solution by the ETSF method has permitted straightforward analyses of the decay kinetics of short-lived cation radicals and the effect of precursor molecules on subsequent reactions. Complex consecutive electron transfer reactions had to be taken into account in the cases described here; conversely, this demonstrates that complex chemical equilibria can be analyzed using the ETSF method.

The dimerization rate constants were determined to be 1.4×10^6 M^{-1} s^{-1} for $MDPA^{\bullet+}$, and 1.0×10^6 M^{-1} s^{-1} for $HDPA^{\bullet+}$. The dimerization rate constant for of $TPA^{\bullet+}$ was determined by the PESF method to be 1.8×10^3 M^{-1} s^{-1}.[7] We can emphasize with the present results that the PESF method could be expanded significantly with newly-accessible reactions by the ETSF method.

To discuss the differences in the reaction rates, we carried out molecular orbital calculations using MOPAC; the optimized structures of the cation radicals were found to be totally different. $TPA^{\bullet+}$ has a propeller-like structure, with "blades" of three equivalent phenyl rings, as reported.[30] Both $MDPA^{\bullet+}$ and $HDPA^{\bullet+}$ have two phenyl rings, the optimized location of which is perpendicular each other for $MDPA^{\bullet+}$, but almost in the same plane for $HDPA^{\bullet+}$. This means that a simple comparison, *e.g.* using the charge density, would be difficult, though the diffusion-controlled electron transfer reactions with $TBPA^{\bullet+}$ were confirmed for all the $TPA^{\bullet+}$, $MDPA^{\bullet+}$ and $HDPA^{\bullet+}$ from the absorption spectra. So, in the present work, it can be only concluded experimentally that the dimerization of $MDPA^{\bullet+}$ is slightly faster than that of $HDPA^{\bullet+}$.

The principle of the ETSF method is very simple. A key point of this method is the use of the long-lived cation radicals ($TBPA^{\cdot+}$, in this work) that permit quantitative electron transfer to initiate the target reactions (the formation of $MDPA^{\cdot+}$ and $HDPA^{\cdot+}$, in this work). Although a redox reagent, such as Cu^{2+}, has been previously used in stopped-flow analysis to generate $TPA^{\cdot+}$,[20] subsequent interaction or complexation with the redox reagent had to be considered in the analysis. Utilizing electron transfer with a bulky oxidant, *e.g.* $TBPA^{\cdot+}$, which would not participate into the follow-up chemical reactions, the ETSF method can be proposed as a useful method for the detection and kinetic analysis of short-lived intermediates.

While the ETSF method is utilized for the analysis of fast dimerization reactions in the present work, the concept of the ETSF method can be further extended, *e.g.* in analyzing fast nucleophilic reactions of cation radicals. That is to say, $TBPA^{\cdot+}$ is sufficiently long-lived[24] that, when the solution is mixed with a solution containing both N [in eqn. (1)] and a nucleophile, the fast reaction of $N^{\cdot+}$ with the nucleophile could be analyzed in a similar manner. These studies are now in progress.

Acknowledgements

One of the authors (M. O.) would like to thank the Mitsubishi Foundation for financial support.

References

1 V. D. Parker, in *Advances in Physical Organic Chemistry*, ed. V. Gold and D. Bethell, Academic Press, London, 1983, vol. 19, p. 131.
2 K. Yoshida, *Electrooxidation in Organic Chemistry*, John Wiley & Sons, Inc., New York, 1984.
3 O. Hammerich and V. D. Parker, in *Advances in Physical Organic Chemistry*, ed. V. Gold and D. Bethell, Academic Press, London, 1984, vol. 20, p. 55.
4 V. D. Parker, *Acc. Chem. Res.*, 1984, **17**, 243.
5 M. S. Workentin, V. D. Parker, T. L. Morkin and D. M. Wayner, *J. Phys. A*, 1998, **102**, 6503 and references therein.
6 M. Schmittel and A. Burghart, *Angew. Chem., Int. Ed. Engl.*, 1997, **36**, 2550.
7 M. Oyama, K. Nozaki and S. Okazaki, *Anal. Chem.*, 1991, **63**, 1387.
8 M. Oyama, K. Nozaki, T. Nagaoka and S. Okazaki, *Bull. Chem. Soc. Jpn.*, 1990, **63**, 33.
9 M. Oyama, K. Nozaki and S. Okazaki, *J. Electroanal. Chem.*, 1991, **304**, 61.
10 M. Oyama, S. Okazaki and T. Nagamura, *Anal. Chim. Acta*, 1991, **245**, 199.
11 M. Oyama, T. Sasaki and S. Okazaki, *J. Electroanal. Chem.*, 1997, **420**, 1.
12 S. Okazaki and M. Oyama, *Curr. Top. Electrochem.*, 1998, **6**, 199.
13 M. Oyama, M. Yamanuki, T. Sasaki and S. Okazaki, *J. Chem. Soc., Perkin Trans. 2*, 2000, 1745.
14 M. Oyama and S. Okazaki, *Anal. Chem.*, 1998, **70**, 5079.
15 M. Oyama, M. Mitani and S. Okazaki, *Electrochem. Commun.*, 2000, **2**, 363.
16 M. Oyama, T. Higuchi and S. Okazaki, *Electrochem. Commun.*, 2000, **2**, 675.
17 A. J. Bard, A. Ledwith and H. J. Shine, in *Advances in Physical Organic Chemistry*, ed. V. Gold and D. Bethell, Academic Press, London, 1976, vol. 13, p. 155.
18 U. Svanholm and V. D. Parker, *J. Chem. Soc., Perkin Trans. 2*, 1973, 1594.
19 R. N. Adams, *Acc. Chem. Res.*, 1969, **2**, 175 and references therein.
20 R. F. Nelson and R. H. Philip, Jr., *J. Phys. Chem.*, 1979, **83**, 713.
21 D. Larumbe, I. Gallardo and C. P. Andrieux, *J. Electroanal. Chem.*, 1991, **304**, 241.
22 H. Yang and A. J. Bard, *J. Electroanal. Chem.*, 1991, **306**, 87.
23 L. Eberson and B. Larsson, *Acta. Chim. Scand. Ser. B*, 1986, **40**, 210.
24 L. Eberson and B. Larsson, *Acta. Chim. Scand. Ser. B*, 1986, **40**, 367.
25 W. Schmidt and E. Steckhan, *Chem. Ber.*, 1980, **113**, 577.
26 G. Cauquis, J. Cognard and D. Serve, *Tetrahedron Lett.*, 1971, **48**, 4645.
27 G. N. Lewis and D. Lipkin, *J. Am. Chem. Soc.*, 1942, **64**, 2801.
28 T. Shida and W. H. Hamill, *J. Chem. Phys.*, 1966, **44**, 2369.
29 M. Oyama, S. Okazaki and T. Nagamura, *Vib. Spectrosc.*, 1991, **1**, 329.
30 J. Pacansky, R. J. Waltman and H. Seki, *Bull. Chem. Soc. Jpn.*, 1997, **70**, 55.